The effect of small embankments on wind speeds

A.D. Quinn[†], A.P. Robertson[‡], R.P. Hoxey,[††] J.L. Short[†] and L.R. Burgess[†]

Environment Group, Silsoe Research Institute, Wrest Park, Silsoe, Bedfordshire MK45 4HS, U.K.

B.W. Smith[‡‡]

Flint & Neill Partnership, 21 Dartmouth Street, London SW1H 9BP, U.K.

Abstract. Full-scale measurements have been made to determine the increase in wind speed over two exposed embankments, one of 23° slope and 4.7 m in height, the other of 24° slope and 7.3 m in height. Measurements were made at heights of 5, 10 and 15 m above the upper edge of each embankment and at the same heights approximately 100 m upwind in the lower-level approach fetch. Despite the modest sizes of the embankments, the maximum recorded increase in mean wind speed was 28% and the minimum was 13%; these increases relate to increases in wind loads on structures erected at the top of the embankments of 64% and 28% respectively. The associated increases in gust speeds are estimated at 33% and 18%, which imply increases in gust loading of 77% and 39% respectively. These experimental results are compared with predictions obtained from a computational fluid dynamics (CFD) analysis, using three high Reynolds number eddy-viscosity models and estimates from the UK wind loading code, BS 6399: Part 2. The CFD results are generally in agreement with the experimental data, although near-ground effects on the embankment crest are poorly reproduced.

Key words: embankment; escarpment; topography; wind speed-up factor; wind loading; computational fluid dynamics; design codes and standards.

1. Introduction

Structures must be designed to resist the wind loading likely to be encountered during their design life. This loading may be exacerbated by the local topography, which causes increases in the local wind speed and hence wind loads (by a factor proportional to the square of wind speed). One type of feature where this may be expected is a road embankment where increased exposure and wind acceleration due to the presence of the embankment may lead to an increased risk of structural failure. These embankments are commonly small when compared with previously

---

† Research Scientist
‡ Senior Research Scientist
†† Head of Group
‡‡ Consultant

studied topographic features such as hills and escarpments but may still produce a significant wind speed-up effect. Increasingly, new road constructions involve sections built on such embankments (to overpass existing roads and to avoid steep gradients), and as a result more lighting columns and other structures are being erected along embankments where they are exposed to these higher wind speeds. Wind loading codes such as the British Standard BS 6399 : Part 2 (BSI 1997) and the Structural Eurocode on wind actions ENV 1991-2-4 (BSI 1997), include topography factors for such features. However, little full-scale information exists to validate the appropriateness of these factors for commonly encountered road embankments. Two full-scale trials have recently been undertaken to assess the wind speed increase. These data are presented here and are compared with computational fluid dynamics (CFD) simulations of the experimental sites and with the relevant wind loading codes (BS 6399: Part 2, ENV 1991-2-4).

2. Methodology

Two embankments of suitable orientation and exposure but different geometry were sought and found. Both were reasonably two-dimensional, were orientated approximately north-south, had a clear lower-level fetch to the west (the prevailing wind direction) and a clear upper-level fetch to the east. For each site, permission was obtained to erect an instrumentation mast in the adjoining field to monitor the approaching reference wind.

2.1. Instrumentation

Measurements were made of total and static pressure at 5, 10 and 15 m heights above the top edge of each embankment and at the same heights above the approach fetch at a position sufficiently far upstream as to be unaffected by the embankment (nominally 100 m). Six directional pitot-static anemometers were prepared for this purpose. A 15 m telescopic, guyed mast was used to support the 3 reference anemometers in the field. Since there was a road running parallel and close to the edge of each embankment, a guyed mast could not be used on the embankments. Instead, a lighting column was adapted and used to support the 3 embankment anemometers. Flexible plastic tubes conveyed the total and static pressure from each anemometer to pressure transducers located at the bottom of each mast and electrical cables conveyed the direction signals. A PC was also located at the bottom of each mast to log all the signals from the mast sensors.

In addition to the reference anemometer mounted at 10 m in the field, a reference static probe was installed at 10 m to provide a common backing pressure for all pressure transducers. A common zero and calibration pressure was applied automatically to all pressure transducers by switching solenoids at the beginning and end of each 20-minute recording period. Synchronised recordings were made at each mast with data being recorded at 6 Hz, although the lengths of pressure transmission tubes used limited the response to 3 Hz. Recordings were made for appropriately strong winds over a range of wind directions around normal to the embankment.

2.2. Embankment sites

Embankment I was 4.7 m high and of a uniform 23° slope (Fig. 1). The fetch consisted of level agricultural land, sown with winter cereal, extending some 500 m upstream to the west
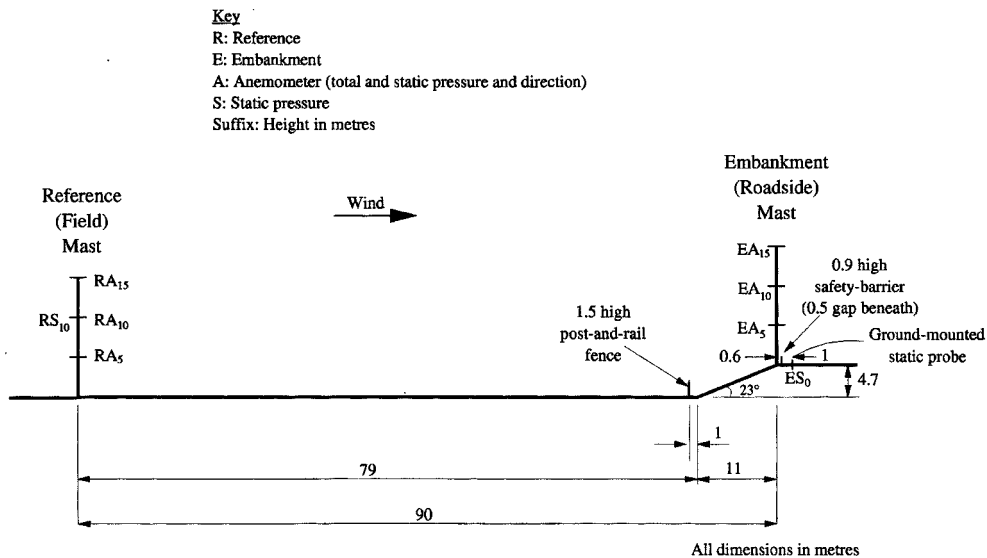
Fig. 1 Layout of Embankment I and instrumentation

on the lower level of the embankment. At the base of the embankment there was a 1.5 m high post-and-rail fence with a solidity of less than 30%. At the top of the embankment was a safety-barrier, 0.9 m high, which consisted of a longitudinal cold formed steel section, supported on substantial timber posts. There was a 0.5 m gap between the horizontal steel section and the ground. On the upper level of the embankment was a 2-lane motorway and access road, giving a total carriageway width of over 25 m. Beyond the carriageway, the terrain remained reasonably flat and unobstructed. The reference mast was positioned 90 m upstream of the embankment. The static pressure was also measured at ground level at the top of the embankment, 1 m downstream
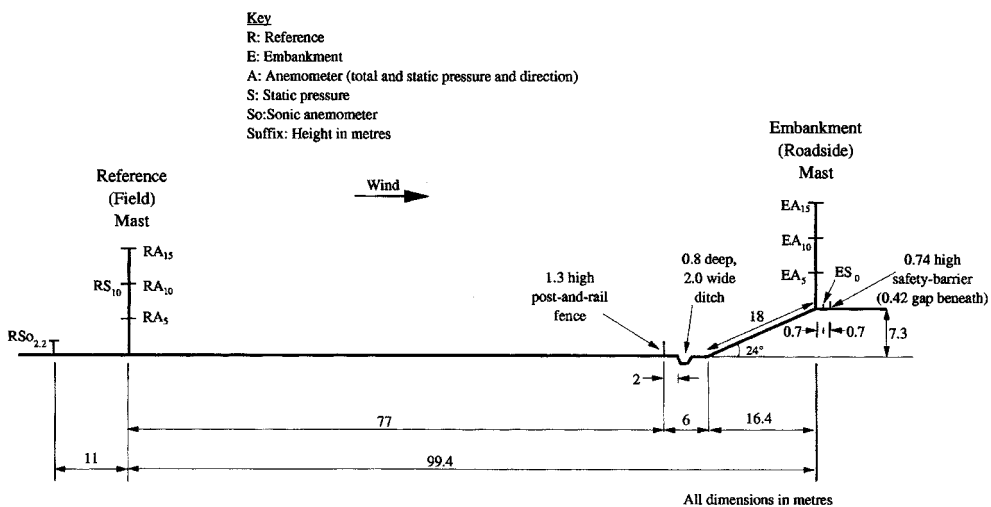

Fig. 2 Layout of Embankment II and instrumentation

of the safety-barrier.

Embankment II was 7.3 m high and of a uniform 24° slope (Fig. 2). The fetch consisted of level agricultural land, covered in straw stubble approximately 150 mm in height, extending some 500 m upstream to the west on the lower level of the embankment. At the base of the embankment there was a 2.0 m wide by 0.8 m deep ditch and a 1.3 m high post-and-rail fence with a solidity of less than 30%. At the top of the embankment was a safety-barrier, 0.74 m high, which consisted of a longitudinal cold formed steel section, supported on steel posts. There was a 0.42 m gap between the horizontal steel section and the ground. On the upper level of the embankment was a 2-lane carriageway and access road, giving a total carriageway width of over 25 m. Beyond the carriageway, the terrain remained reasonably flat and unobstructed. The reference mast was positioned 99.4 m upstream of the embankment. A sonic anemometer was positioned a further 11.0 m upstream at a height of 2.2 m to provide additional data on the approaching wind speed and direction and to enable the friction velocity, $u*$, to be determined. The static pressure was also measured at ground level at the top of the embankment, 0.7 m upstream of the safety-barrier.

2.3. Computational study

The experimental sites were also studied using a computational fluid dynamics (CFD) package (CFDS CFX 4.1) incorporating three high Reynolds number k-ε turbulence models. These were the standard k-ε model (Launder and Spalding 1974), the RNG k-ε model (Yakhot and Orzag 1986) and the MMK k-ε model (Tsuchiya *et al.* 1997). The inlet boundary wind profile was specified to give a logarithmic mean velocity profile and self sustaining turbulence profile given a constant roughness length on the ground surface of 0.01 m. The numerical schemes used were second order (high order upwind differencing) or third order (quadratic differencing) accurate according to the best scheme available for the turbulence model in use.

The simulation solution domain for this study extended 100 m upwind and 100 m downwind of the embankments and was a minimum of 50 m in depth. Three grids were used to assess the grid effects, these ranged from 68×35 with a near ground cell size of 0.1 m to 232×105 with a near ground cell size of 0.033 m. The surface roughness, of 0.01 m, was maintained across the entire domain in order to maintain the velocity profile correctly and obstructions (fences etc.) were explicitly included.

The standard k-ε turbulence model used in this study has been widely used in many CFD studies and has proved to be a robust model with, however, a tendency to incorrectly predict flows close to bluff bodies. As a result, a number of modifications to it have been proposed, two of which, the RNG and MMK models, have been shown to be more appropriate in certain wind engineering studies (Tsuchiya *et al.* 1997).

2.4. Wind loading codes

A number of wind loading codes contain provisions to account for the effect of topography on wind speeds. These include BS 6399 : Part 2 (BSI 1997) and ENV-1991-2-4 (BSI 1997) which are equivalent in describing the topography factor in terms of a topographic location factors s and an effective slope parameter ψ_e. In the "Standard" methods of both these codes, these factors are combined in the term $1.2\ \psi_e s$ which is added to the altitude factor to give a

correction to the basic site wind speed. In BS 6399 : Part 2 there is also an alternative method, the "Directional" or "Full" method, which uses the term 2.0 $\psi_e s$ applied to the individual wind directions, the effects of which are then summed. These codes are supposed to provide an upper bound estimate of gust loading on structures for design purposes.

Previous work on flow over ridges and embankments (Bowen 1983), based on the work of Hunt (1980), has also quantified the effects of large (~1000 m) topographic features such as hills and ridges. This describes the flow over similar 2D embankments in terms of the "inner" and "outer" layers of the flow and provides equations such as Eq. (1) for the "outer" layer, where $\sigma(z)$ is the fractional speed-up factor at vertical height z above the crest of an embankment with effective length L.

$$\sigma(z) = \frac{1}{2\pi} \ln \left(\frac{1 + \left(\dfrac{z}{L} \right)^2}{\left(\dfrac{z}{L} \right)^2} \right) \tag{1}$$

This is related to the "loading" speed-up factor (the square root of the wind loading multiplier) by Eq. (2) where $u(z)$ is the wind speed at height z above the local ground, u_{ref} is the velocity profile of the upstream flow at a reference position and H is the effective height of the embankment.

$$\frac{u(z)}{u_{ref}(z)} = \frac{\dfrac{H}{L} \sigma(z) u_{ref}(L) + u_{ref}(z)}{u_{ref}(z)} \tag{2}$$

This "outer" layer is defined at being above a height l given by Eq. (3).

$$l \ln \left(\frac{l}{z_0} \right) = 2 \kappa^2 L \tag{3}$$

where κ is von Karmans constant (0.41) and z_0 is the surface roughness length. Since, for both the cases reported here, $l < 1$ m, the "inner" layer has not been considered further.

3. Results

The data collected at Embankment I consisted of nine 20-minute records made during April 1996 for winds with a mean speed of approximately 6.5 m/s at the 10 m reference position and with directions approximately normal to the embankment. At Embankment II, fifteen 20-minute records were collected in October 1996 for winds with a mean speed of approximately 9 m/s at the 10 m reference position and with mean directions from 5° to 50° from normal to the embankment. Unfortunately, between the date the instrumentation masts were erected and the date recordings were made, the 15 m reference anemometer at Embankment II was rendered inoperable, apparently as a result of avian-inflicted damage to the vane arm.

Table 1 Mean velocity profile factors at reference masts with respect to 10 m reference mean velocity

Height (m)	Profile at Reference Mast (Embankment I)	Profile at Reference Mast (Embankment II)	CFD Profile (Boundary Condition)
2.2	-	0.71	0.78
5	0.91	0.90	0.90
10	1.00	1.00	1.00
15	1.05	-	1.06

Table 2 Static pressures (C_p) measured and predicted at the embankment crest

Embankment	Height (m)	Measured	Standard $k\text{-}\varepsilon$	MMK $k\text{-}\varepsilon$	RNG $k\text{-}\varepsilon$
I	0	-0.74	-0.93 / -1.04*	-0.82 / -0.98*	-1.11
	5	-0.33	-0.34*	-0.28 / -0.33*	-0.35
	10	-0.32	-0.26*	-0.24 / -0.26*	-0.26
	15	-0.30	-0.22*	-0.23 / -0.24*	-0.22
II	0	-0.39	-0.83	-0.70	-0.75
	5	-0.50	-0.52	-0.49	-0.52
	10	-0.39	-0.41	-0.40	-0.41
	15	-0.41	-0.35	-0.35	-0.35

*The range indicates the results obtained from the 3 numerical grids used.

These data have been analysed to give mean and gust speed-up factors, and turbulence intensities as well as normalised static pressure differences at the top of the embankment. Spectral analysis of the results has also been undertaken.

The velocities collected from the upstream reference masts are summarised in Table 1 which also contains the boundary conditions used in the CFD simulations. These measured boundary conditions compare well with the log-law velocity profile, based on a surface roughness of 0.01 m as used in the CFD. Turbulence data collected gave consistent turbulence intensities of 20%~23% at all heights both at the reference mast and on the embankment at both sites. The CFD boundary conditions represent this profile and include self sustaining turbulence levels, which are considered representative of the high frequency component of atmospheric turbulence, in line with the work of Richards and Hoxey (1993).

The mean static pressure at the crest of each embankment is given in Table 2, together with the predictions from each of the CFD models used. The data are presented as pressure coefficient (C_p) values with reference to the 10 m measurements on the upstream reference mast. Ranges are presented for the cases where a CFD model has been used with each of the three numerical grids described above. In some combinations these variations made no difference to the results of static pressure and these are denoted in the table by single-value ranges.

The increases in mean velocity measured at Embankments I and II are presented in Figs. 3 and 4 respectively as mean velocity ratios (embankment velocity divided by the upstream reference velocity recorded at the corresponding height). In each case, the ratios presented are those for an approximately perpendicular wind direction, although from the data collected at Embankment II it was found that the ratios reduced slightly over the 45° range of glancing winds for which measurements were made. Also shown in these figures are the results of the three CFD models tested and the mean speed-up predicted by BS 6399 : Part 2 (which is
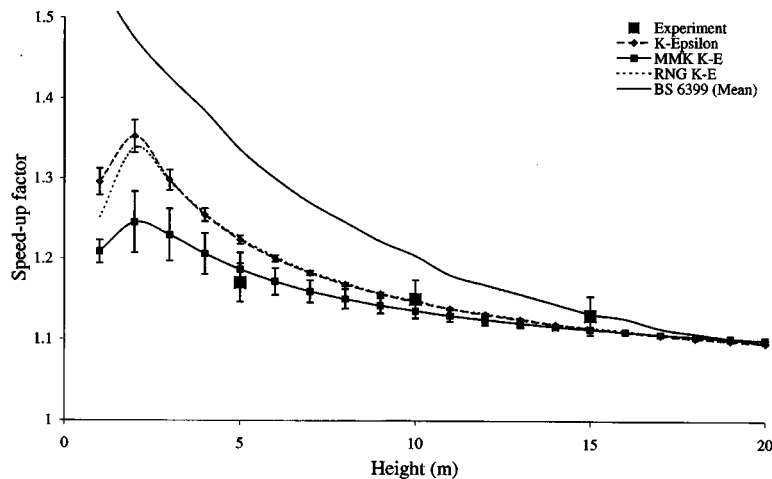
Fig. 3 Mean speed-up ratios for Embankment I : comparison of measured and CFD values
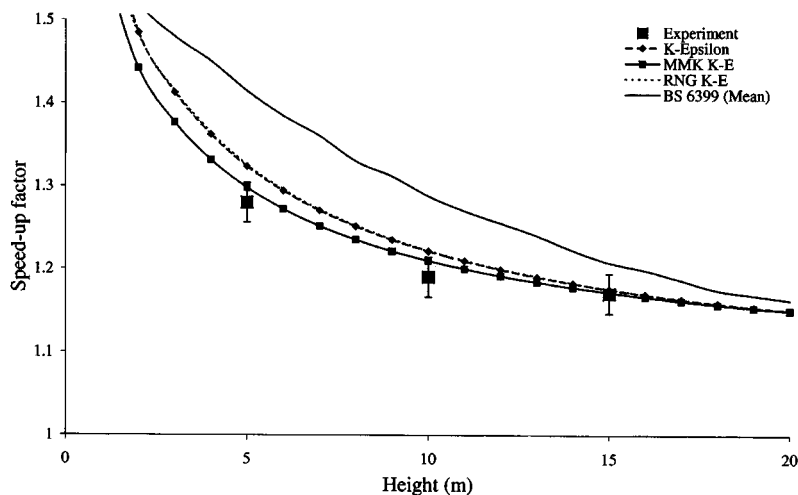

Fig. 4 Mean speed-up ratios for Embankment II : comparison of measured and CFD values

equivalent to ENV 1991-2-4). In the case of Embankment I (Fig. 3), the standard k-ε and MMK k-ε results are given bounds of error due to grid effects using the three numerical domains outlined above. The trend with increasing refinement of the grid depended on the model in use. The results of the standard k-ε model increased with grid refinement, whereas those of the MMK k-ε model decreased. These effects where, however, confined to areas near the ground and the basic grid has therefore been considered adequate for comparison purposes.

Figs. 5 and 6 summarise the results obtained from the measurements, the CFD and the BS 6399 : Part 2 (both the "Standard" method, which is equivalent to ENV 1991-2-4 and the "Full" or "Directional" method) estimates when expressed as a gust speed increase factor. In order to convert the CFD results, which are fundamentally mean increase factors, to gust increase factors, the methodology of Paterson and Holmes (1993) has been adopted. This uses the calculated values for mean speed increase and the turbulence statistics provided by the
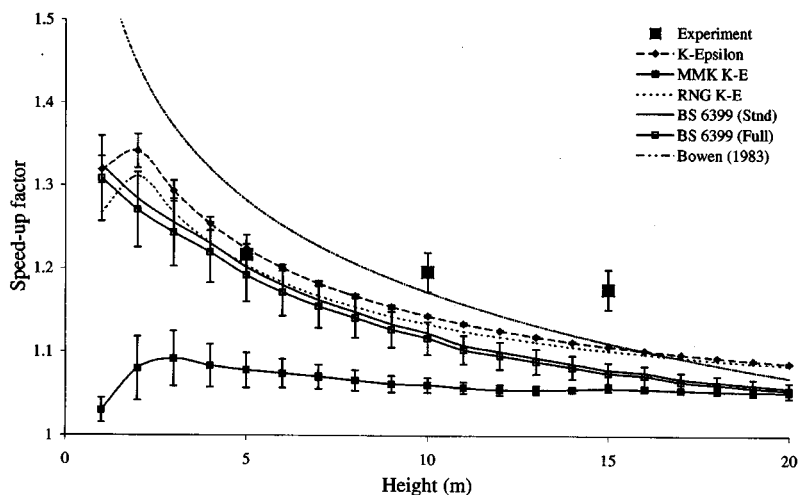
Fig. 5 Gust speed-up ratios for Embankment I : comparison of measured CFD results with design code values and the results of Bowen (1983)
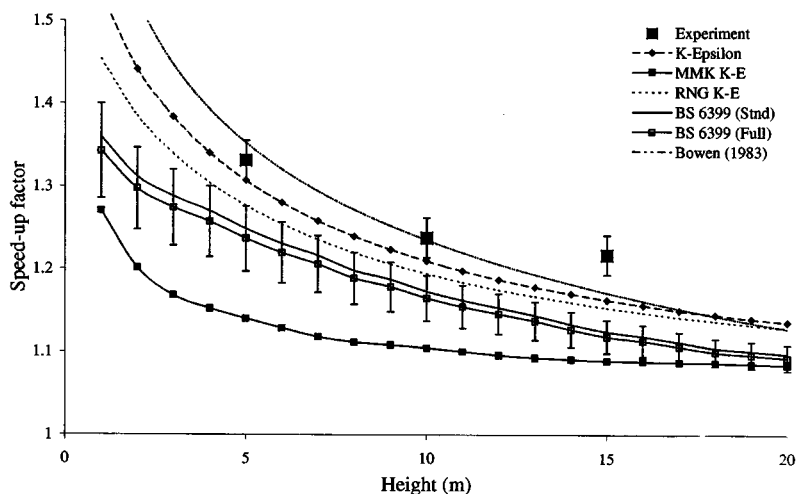

Fig. 6 Gust speed-up ratios for Embankment II : comparison of measured and CFD results with design code values and the results of Bowen (1983)

CFD results to give a gust speed increase factor according to Eq. (4).

$$\hat{u} = \bar{u} + 3.7\sqrt{\overline{u^2}} = \bar{u} + 4.055\sqrt{k} \qquad (4)$$

where $\hat{u}$ is the gust wind speed and k is the turbulent kinetic energy. In addition Figs. 5 and 6 also display the results of the study by Bowen (1983), as given in Eqs. (1) and (2), scaled to the appropriate sizes.

In these figures, the data are presented as gust speed-up factors, in line with the design code methodologies. The values given for BS 6399 : Part 2 ("Full" method) are given bounds of values associated with the various other parameters involved in this code methodology.
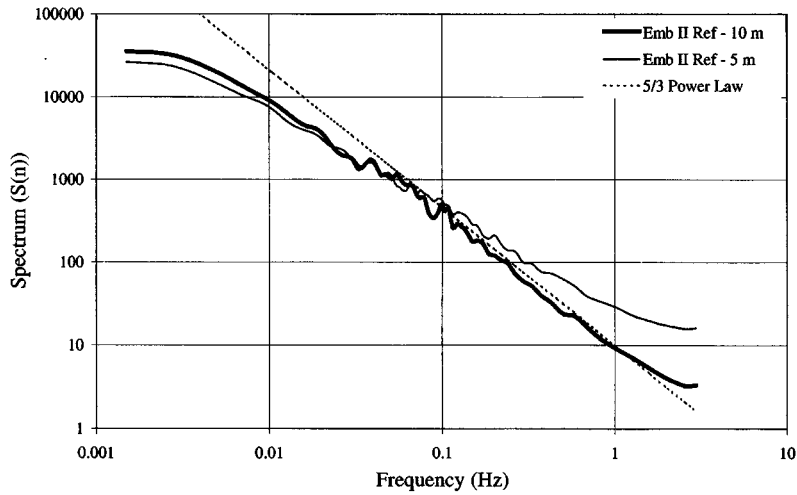
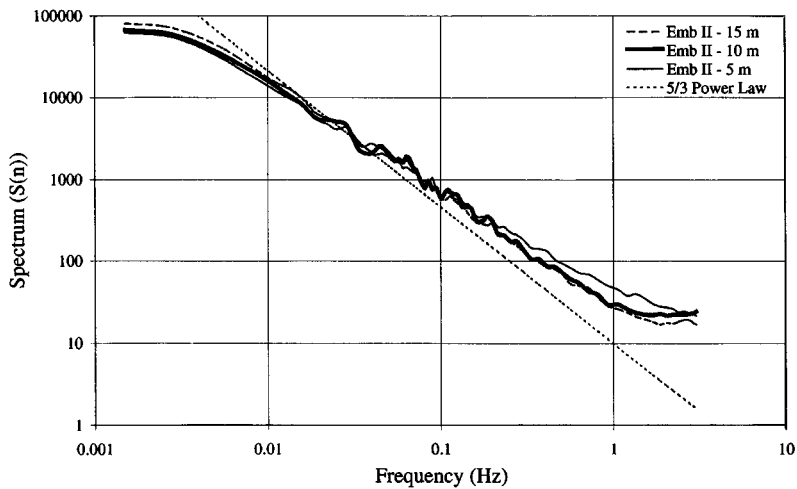Fig. 7 Spectra from reference mast data : Embankment II

Fig. 8 Spectra from embankment mast data : Embankment II

These indicate the range of possible values one might obtain given different exposures of location (within the UK). The experimental values presented have been obtained by applying an estimate of the gust factor obtained from the measurements to the mean values. The value of this factor is 1.04 ± 0.03 and is derived from the gust-to-mean velocity ratios observed at all heights for both embankments.

A spectral analysis of the data collected during the experiments has also been undertaken. The spectra obtained from the reference mast of Embankment II is shown in Fig. 7. The equivalent data from the embankment mast is given in Fig. 8. The speed-up factor can also be expressed in the frequency domain by the fourth root of the ratio of the embankment and reference spectra. These are presented in Fig. 9 for Embankment II. The data for Embankment I gave similar results although, because of the shorter duration of the data (nine 20 minute records instead of the 15 records at Embankment II), the noise level is proportionally higher.
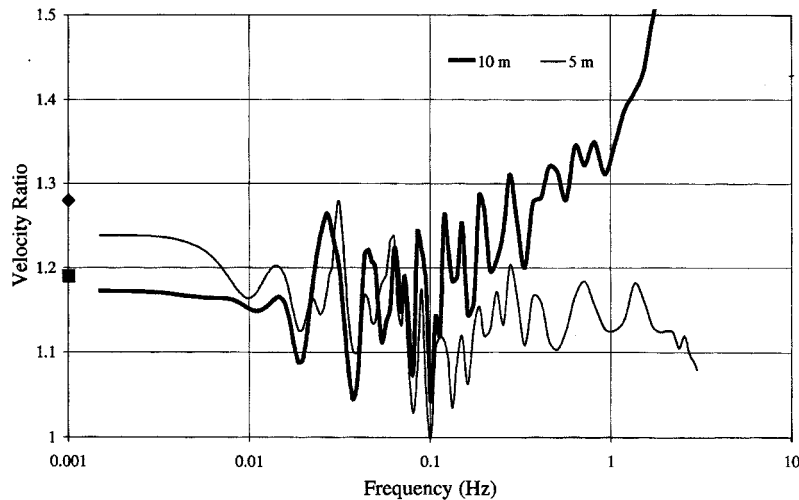
Fig. 9 Frequency domain plot of speed-up ratio with mean speed-up ratio indicated by the symbols on the left of the polt

4. Discussion

The prediction of mean speed-up ratio directly by CFD codes based on eddy-viscosity turbulence models, such as the ones used in this study, has been questioned (Zeman and Jensen 1987) because of the well known problems of predicting turbulence generation and suppression under conditions of streamline curvature. The results of this study suggest that for small embankments (<10 m vertical height), this may not be a significant problem, except very close to the ground. Indeed, the MMK variant of the k-ε model seems to correctly predict the measured speed-up ratios in both cases. The difference between the other two models used is not significant in this case.

When the turbulence levels are included, Figs. 5 and 6, to provide gust speed-up ratios, the differences in the models is, as would be expected, more pronounced. The reason for this is that in both cases the modifications to the standard k-ε model have reduced the generation of turbulence at the leading edge of bluff bodies. Eq. (4) translates this difference in turbulence levels into differences in the gust speed-up ratio. The more effective of the models at reducing this over production of turbulence, the MMK model, therefore produces the lowest gust speed-up ratios.

The comparison of these CFD results with the experimental data is, however, not as straightforward as may first appear from these figures. This is due to the general "under-prediction" of turbulence by CFD in atmospheric boundary layer (ABL) simulations of this type. Richards and Hoxey (1993) have explained this in terms of the spectral content of ABL turbulence and that CFD codes in fact reproduce only a small (high frequency) fraction of this based on the grid size used in the calculations. The apparent under-prediction of gust speed-up ratio by the MMK model may, therefore, be more satisfactory, being of the correct trend over the vertical range, than the more apparently correct standard k-ε and RNG models which do not behave correctly over the height range considered in each case. None of these

models, however, reproduces the correct proportional increase in turbulence seen in the measurements. Figs. 3 and 5 indicate that the grid resolution of these calculations is also important as the ground is approached, but a 300% increase in grid resolution in this case produced differences in results near the ground of only the same magnitude as the experimental error and much less at higher levels. It is interesting to notice that the inclusion of the turbulence term in the calculation of the gust speed-up ratio has the effect of reducing the grid effects in each case.

The effect on the static pressure predictions at and above the embankment crest follows the same pattern as the velocity results, the discrepancies being most pronounced at ground level. Table 2 shows the results for static pressure from the two embankments and it can be seen that in all the CFD cases the ground level suction is over-predicted. This and the associated velocity discrepancies near ground level, are considered to be due to the lack of a recirculation zone at the crest of each embankment in the CFD simulations, where one was observed (visually) during the experiments. The enhanced static pressure (suction) predicted at the crest in the simulations is consistent with this and is necessary to keep the flow attached. Above this region, the predictions become more reasonable but, as with the velocity values, tend to under-predict static pressure as height increases. Since, in this type of CFD code, the pressure is derived from the velocity field calculation, this is unsurprising but highlights the need for careful definition of pressure boundary conditions in external flow simulations.

The experimental results themselves are interesting because of the apparent lack of variation with height that might be expected given the results from larger topographic features (Bowen 1983). However if the results are replotted on a non-dimensional scale (Fig. 10), it can be seen that there is consistency across the two cases. This suggests that for small embankments, the reduction of speed-up ratio with height is not as rapid as would be inferred from data on larger scale features. Certainly the current design codes appear to under-estimate the gust speed-up factors observed in these cases, although this may be accounted for by the over-estimation of other related terms in the design codes. There is, however, little difference between the observed values of mean and gust speed-up factors (a ratio of 1.04±0.03), which suggests that this
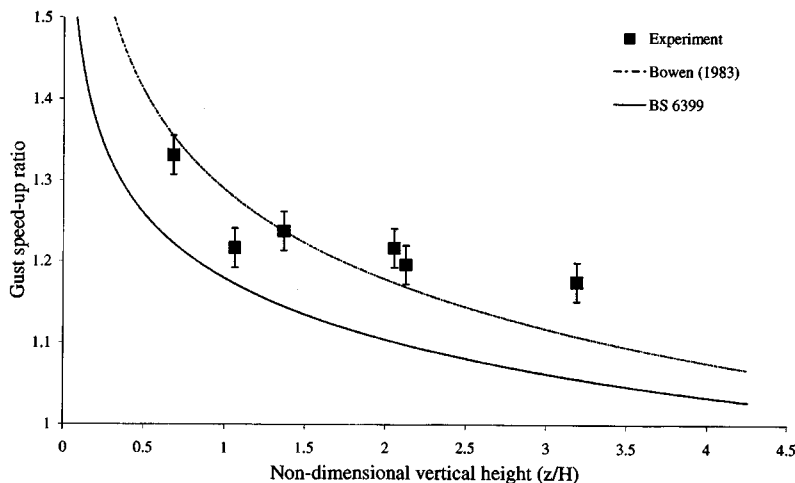

Fig. 10 Gust speed-up ratios for both embankments as a function of non-dimensionalised vertical height

discrepancy is not due to the type of extreme value analysis used.

The design codes included here appear to over-estimate the mean speed-up factor observed in these small embankments (Figs. 3 and 4) for positions <15 m, whilst at the same time under-estimating the gust contribution (Figs. 5 and 6). This may be compensated for in other sections of the design code, but suggests that the wind speed description may need revising for small sharp embankments such as these.

The spectral analysis of the reference mast data from both sites is generally as would be expected, with a noticeable reduction in turbulent length scale as the ground is approached (Fig. 7). The effect of the embankment is also apparent, with the overall reduction in length scale visible in Fig. 8. Turbulence levels also rise at the crest of the embankment, although this is balanced by the increase in velocity, hence the constant turbulence intensity results. The spectral analysis of the speed-up ratio (Fig. 9), however, shows an interesting difference between the responses at different heights. The lower (5 m) measurements, with highest overall speed-up ratio, have an approximately equal contribution from across the frequency range, whereas the higher station has a significant contribution from the speed-up of the higher frequency gusts. This again suggests that the streamline curvature effect on turbulence in this case is confined to the region <5 m.

5. Conclusions

The measurements of wind velocity profile indicate that topography effects are significant even with relatively small (<10 m vertical height) embankments. The change in magnitude of speed-up factor with height is not well represented by BS 6399 : Part 2, which over-estimates the *mean* speed-up factor but under-estimates the *gust* speed-up factor for these small embankments, nor is it well represented by the scaling down of the results from larger topographic features. CFD predictions are in line with the measurements of *mean* speed-up factors, which is consistent with the methodology of CFD simulation. However, when turbulence parameters are used to infer *gust* speed-up ratios, the results are less clear because of the discrepancy in the prediction of turbulence in eddy-viscosity models when compared to ABL turbulence. CFD also tends to over-predict the negative static pressure at ground level due to an inability to resolve the flow detail, i.e., the separation, in this region.

Acknowledgements

References

Bowen, A.J. (1983), "The prediction of mean wind speeds above simple 2D hill shapes", *J. Wind Eng. Ind. Aero.*, **15**, 259-270.

BS 6399 : Loading for buildings : Part 2 : Code of practice for wind loads : 1997. British Standards Institution, London.

ENV 1991-2-4 : 1995 Eurocode 1 : Basis of design and actions on structures. Part 2.4 Actions on structures-Wind actions. 1997. British Standards Institution, London.

Hunt, J.C.R. (1980). Wind over hills, in *Workshop on the planetary boundary layer*, 107-149, J.C. Wyngaard (ed), American Meteorological Society, Boston.

Launder, B.E. and Spalding, D.B. (1974), "The numerical computation of turbulent flows", *Comput. Methods Appl. Mech. Eng.*, **3**, 269-289.

Paterson, D.A. and Holmes, J.D. (1993), "Computation of wind flow over topography", *J. Wind Eng. Ind. Aero.*, **46-47**, 471-476.

Richards, P.J. and Hoxey, R.P. (1993), "Appropriate boundary conditions for computational wind engineering models using the k-ε turbulence model", *J. Wind Eng. Ind. Aero.*, **46-47**, 145-153.

Tsuchiya, M., Murakami, S. Mochida, A., Kondo, K. and Ishida, Y. (1997), "Development of a new k-ε model for flow and pressure fields around bluff body", *J. Wind Eng. Ind. Aero.*, **67-68**, 169-182.

Yakhot, V. and Orszag, S.A. (1986), "Renormalization group analysis of turbulence", *Journal of Scientific Computing*, **1**(1), 3-51.

Zeman, O. and Jensen, N.O. (1987), "Modification of turbulence characteristics in flow over hills", *Q. J. R. Meteorol. Soc.*, **113**, 55-80.

(Communicated by Giovanni Solari)